One-dimensional model of yeast prion aggregation

K. C. Kunes, D. L. Cox, and R. R. P. Singh
Department of Physics, University of California, Davis, California 95616, USA
(Received 3 May 2005; revised manuscript received 14 July 2005; published 9 November 2005)

Mammalian prion proteins (PrP) are of significant public health interest. Yeasts have proteins, which can undergo similar reconformation and aggregation processes to PrP, without posing a threat to the organism. These yeast "prions," such as SUP35, are simpler to experimentally study and model. Recent *in vitro* studies of the SUP35 protein found long aggregates, pure exponential growth of the misfolded form, and a lag time which depended weakly on the monomer concentration. To explain this data, we have extended a previous model of aggregation kinetics along with a stochastic approach. We assume reconformation only upon aggregation and include aggregate fissioning and an initial nucleation barrier. We find that for sufficiently small nucleation rates or seeding by a small number of preformed nuclei, the models achieve the requisite exponential growth, long aggregates, and a lag time which depends weakly on monomer concentration. The spread in aggregate sizes is well described by the Weibull distribution. All these properties point to the preeminent role of fissioning in the growth of misfolded proteins.

DOI: 10.1103/PhysRevE.72.051915 PACS number(s): 82.39.Fk

I. INTRODUCTION

Bovine spongiform encephalopathy (BSE) in cows, Scrapies in sheep, Creutzfeldt-Jakob Disease (CJD) and Kuru in humans are all diseases caused by a specific misfolded protein residing on neurons [1,2]. This prion protein (denoted PrP^c in its normal form and PrP^{sc} in its misfolded form) is present in all mammals and its full function, to date, is still unknown. A growing body of evidence strongly implies that this disease propagates not by nucleic acids, such as DNA or RNA, but by misfolded proteins (PrP^{sc}) [3,4]. In our current understanding of prion diseases, the autocatalytic misfolding of the prion proteins plays a central role. The misfolded form PrP^{sc} entices normal versions of the cellular prion protein (PrP^c) to change conformation to the misfolded or disease causing form. Although PrP^c and PrP^{sc} have the same amino acid sequence (230 amino acids or residues), PrP^{sc} has a higher beta sheet content than its normal form [1]. In humans, the disease is mostly sporadic, perhaps caused by a rare spontaneous misfold of the protein. But, infectious forms are also known to occur, such as in the case of new-variant CJD caused by eating BSE infected meat. In the latter case, infectious agents are presumably misfolded "seeds" that have entered the body from outside. Developing an understanding of the misfolding process should provide insights to prevention and/or cure of these diseases.

A class of proteins in yeast (SUP35) undergo a conformation change similar to the mammalian PrP. However, in case of yeast, this does not kill the organism. In fact, reconfigured, aggregated forms lead to a new phenotype [5]. Because they are not toxic, the misfolding is much easier to study for these proteins. Besides, it has been shown that aggregates produced *in vitro* can lead to the same phenotype, when added to a yeast cell [6–8]. Thus, it is possible to study the molecular aggregation processes for yeast prions in a test tube in tremendous detail, and a large quantity of experimental data is indeed available [9,10].

In this paper, we explore, using conventional kinetic as well as stochastic models, the aggregation dynamics for model yeast prions with a particular goal of explaining *in vitro* data [9,10] including (i) linear aggregates which grow by monomer addition, (ii) a modest concentration dependence of initial aggregate growth time varying roughly inversely as the square root of the monomer concentration, (iii) an observed distribution of aggregate sizes with a mode that is large ($10s-100s$ of monomers), and (iv) a sigmoidal growth that is nearly exponential. We extend the nucleation and fissioning model of Collins *et al.* [9,10] from a moments-only model to monitor individual polymer lengths and show that we can readily obtain the above listed features in the data. In particular, we argue against a model based upon rapid equilibration with micelles, which can also provide a weak concentration dependence to initial aggregation times [11,12], but not the exponential growth implied by including explicit fission of aggregates. The fission rate plays a central role in determining the time scales as well as the mean aggregate length. The range of aggregate sizes assumes a Weibull distribution, also well known from other processes where fissioning is important. Thus the agreement with experiments highlights the importance of fissioning in the growth dynamics.

We study our kinetics both with continuous time modeling and via the discrete time stochastic Gillespie algorithm. The motivation for applying the latter is to determine where stochastic effects from the relatively rare processes of large length polymer generation may be observable in experiment.

In considering the relevance of these studies to mammalian prions, there is an important caveat that arises from the fact that mammalian prions are glycosyl phosphatidylinositol (GPI) anchored on neuron cells and, thus, move in a two-dimensional plane and, hence, can lead to areal aggregates [13,14]. The aggregation and fissioning processes are likely to be very different there. Nevertheless, the dominance of fissioning can lead to long-time growth kinetics, which are in many ways closely related.

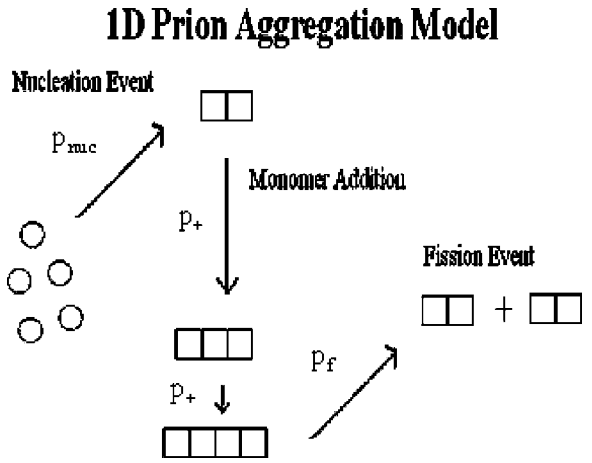

FIG. 1. Aggregation model where circles are normal proteins (psi^-) and squares are the misfolded type [PSI^+].

II. MODELS

We consider a one-dimensional aggregation model that includes a nucleation barrier, elongation by monomer addition, and fission (Fig. 1). The same kind of kinetics was considered by Collins *et al.* in the form of moments of the full polymer kinetic equations, but not in the explicit length resolved form considered here [9,10]. The assumption that monomer (rather than oligomer) addition dominates and the need for fission are underscored by the data we seek to describe on yeast prions [9,10]. We shall distinguish the model quantitatively from a nonfission based model later in the paper.

A nucleation event occurs very rarely and is composed of two normal [psi^-] proteins interacting in such a way that a misfold occurs and they bind together; this two prion aggregate is called a [PSI^+] dimer. The actual size of the nucleus is not a critical parameter in our model, as long as the nucleation process is much slower than aggregation. Once an aggregate has been created, it can elongate by monomer addition. Our model does not consider fusion between two oligomers. The rate of fissioning becomes important only when an oligomer of large enough size arises. After an oligomer has fissioned into smaller pieces, the individual pieces can grow and fission. When a fission leads to a monomeric product, we assume that it returns to the properly folded state. This process leads to a steady state distribution of oligomer sizes and a pure exponential growth. It continues until the monomer concentration begins to dwindle significantly.

We note that the lag time for the *in vitro* growth of yeast prion-like proteins is reproducible in experiments, and shows a weak dependence on monomer concentration. Hence, it is not likely that it can be associated with pure nucleation (at least at low initial monomer concentration), which being a rare event will lead to a distribution of time scales as well as a rather strong dependence on monomer concentration, depending on the size of the nucleus. We will assume that the lag time arises from the growth of misfolded material to an observability threshold. This assumption is valid if the nucleation time scales, which are long compared to other microscopic time scales, are still shorter than this latter time scale. It is also valid when a small number of nucleated seeds exist at the time of the preparation of the experimental samples. As shown elsewhere, a weak concentration dependence to lag time can derive from rapid equilibration of monomer concentration with nonfibrillar oligomers [11,12]; this model is not supported in the current context, and we shall discuss this later in this section.

A. Kinetic model

Our first approach is to use kinetic equations to describe the aggregation process [15,16]. In order to use the rate equations, one must assume a large number of monomers. The kinetic rate equations for our model are as follows

$$\frac{dn_1}{dt} = -2p_{nuc}n_1^2 - 2p_+n_1\sum_{i=2}^{N-1} n_i + 2p_f\sum_{i=2}^{N-1} n_i, \tag{1}$$

$$\frac{dn_2}{dt} = p_{nuc}n_1^2 - 2p_+n_1n_2 - p_fn_2 + 2p_f\sum_{i=3}^{N-1} n_i, \tag{2}$$

$$\frac{dn_k}{dt} = 2p_+n_{k-1}n_1 - 2p_+n_kn_1 - (k-1)p_fn_k + 2p_f\sum_{i=k+2}^{N-1} n_i, \tag{3}$$

$$\frac{dn_N}{dt} = 2p_+n_{N-1}n_1 - p_f(N-1)n_{N-1}, \tag{4}$$

where n_1 is the monomer concentration, n_k is the concentration of k-mers, and N is the longest oligomer kept in the calculation. The parameters p_{nuc}, p_+, and p_f can be adjusted to change the rate of nucleation, fusion, and fission, respectively. Since one of these parameters can be absorbed into the definition of the time t, we will set $p_+=1$. Furthermore, we will set the initial monomer concentration to unity. The equations listed above form a system of N-coupled differential equations which cannot be solved analytically because of the nonlinear terms.

An analytical solution is possible if n_1 can be assumed to be a constant and n_2 and higher are much, much smaller than the monomer concentration. Then the set of equations become linear and can be solved by several techniques, such as a Laplace transformation. This is not a bad approximation, for, as we will see, during much of the growth process the monomer concentration is nearly constant. Only at the end, the monomer concentration begins to dwindle and the amount of misfolded monomers saturates. It is useful to define the zeroth and first moments of the aggregate size distribution as

$$A = \sum_{i=2}^{N} n_i, \tag{5}$$

$$M = \sum_{i=2}^{N} i * n_i, \tag{6}$$

where A is the number of polymer aggregates and M is the total number of monomers in aggregate. Since the overall number of proteins is conserved, the rate of change of M is given by

$$\frac{dM}{dt} = -\frac{dn_1}{dt}, \tag{7}$$

whereas the rate of change of A is given (ignoring the cutoff N) by the equation

$$\frac{dA}{dt} = p_{nuc} n_1^2 - p_f n_2 + p_f \sum_{i=3} (i-3) n_i. \tag{8}$$

If we ignore the terms depending on n_2 and assume n_1 is a constant, we get two linear coupled equations,

$$\frac{dA}{dt} = \text{const} + p_f M - 3 p_f A, \tag{9}$$

$$\frac{dM}{dt} = \text{const} + (2p_+ n_1 - 2p_f) A. \tag{10}$$

We set $p_+ = 1$ to set the unit of time. Anticipating $M \gg A$, which means that the mean aggregate size is much bigger than unity. The above equations mean that the M and A both grow exponentially as $e^{\lambda t}$, with λ given by

$$\lambda = \sqrt{2p_f(n_1 - p_f)} \approx \sqrt{2p_f n_1}. \tag{11}$$

During the exponential growth, the mean aggregate size is given by

$$\bar{L} = \frac{M}{A} = \sqrt{\frac{2n_1}{p_f}}. \tag{12}$$

If we further assume that the lag time is given by the time it takes for the misfolded proteins to reach a detectable threshold M_f, then the lag time is given by

$$t_{lag} \sim \frac{\ln \dfrac{M_f}{C(n_1)^2}}{\sqrt{2p_f n_1}}, \tag{13}$$

where C is a constant and the n_1 dependence inside the logarithm comes from the prefactors. We will see that these results are confirmed by a complete numerical integration of the differential equations. Thus, this model demonstrates the requisite t-lag dependence seen in the experimental data, namely the inverse square root dependence on the monomer concentration, up to logarithms, shown in Fig. 2. We note that the fit in Fig. 2 is not sensitive to the logarithmic terms.

Kinetic model results

A numerical integration approach was used to study the full set of equations. We used the fourth order Runge-Kutta algorithm for solving differential equations and to obtain length distributions and growth curves for the system.

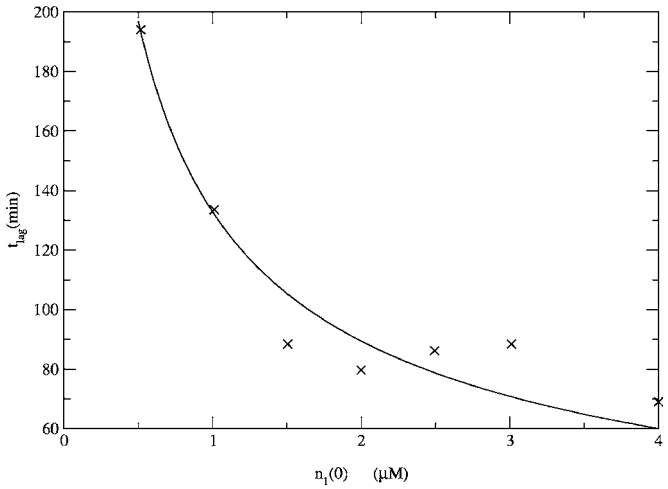

FIG. 2. Lag time (t_{lag}) vs initial monomer concentration $[n_1(0)]$. The crosses are data from Collins *et al.* in Ref. [9]. The continous curve is a fit to the equation $t_{lag} = a_0 [n_1(0)]^{-1/2} \log a_1/n_1(0)$, with $a_0 = 9.22\ min * (\mu M)^{1/2}$ and $a_1 = 1.80 \times 10^6 \mu M$, following Eq. (13).

In Fig. 3, we show plots of $\log(M)$ as a function of time. We have chosen a set of parameters yielding mean lengths in the $10s - 100s$ and displaying manifest exponential growth in $M(t)$ vs t plots. It is evident that there is a regime where $\log(M)$ varies linearly with time, implying a pure exponential growth. This region of exponential growth is not limited to just a few chosen parameter values, but can be achieved over a wide range of p_f values. In Fig. 3, we plot the total number in aggregate vs time, now on a linear scale. The sigmoidal growth is now evident as the exponential increase tapers off when the monomers begin to deplete. This is also consistent with the experimental results [9].

As discussed earlier, the mean length of the aggregates has a simple inverse square-root dependence on the rate of fission. Thus by tuning the rate of fission, it is possible to obtain mean aggregate lengths (see Fig. 4), which appear

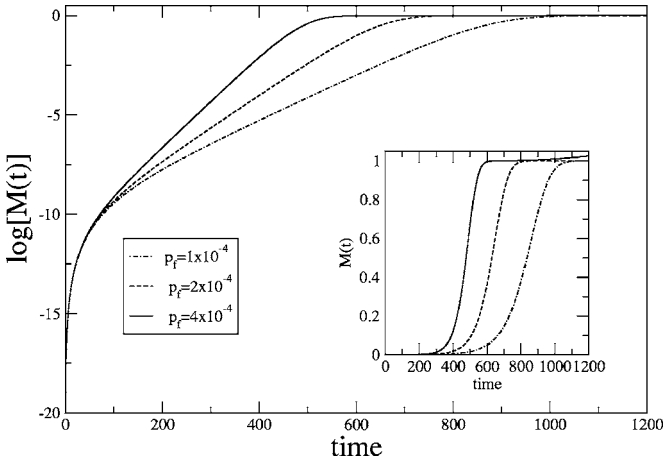

FIG. 3. Log$[M(t)]$ vs time, with parameter values $n_1(0) = 1$, $p_+ = 1$, $p_{nuc} = 10^{-8}$. The linear regions illustrate regions of pure exponential growth. $M(t)$ vs time illustrating sigmoidal growth is shown in the inset. Note that time is in units of $1/[n_1(0)p_+]$.

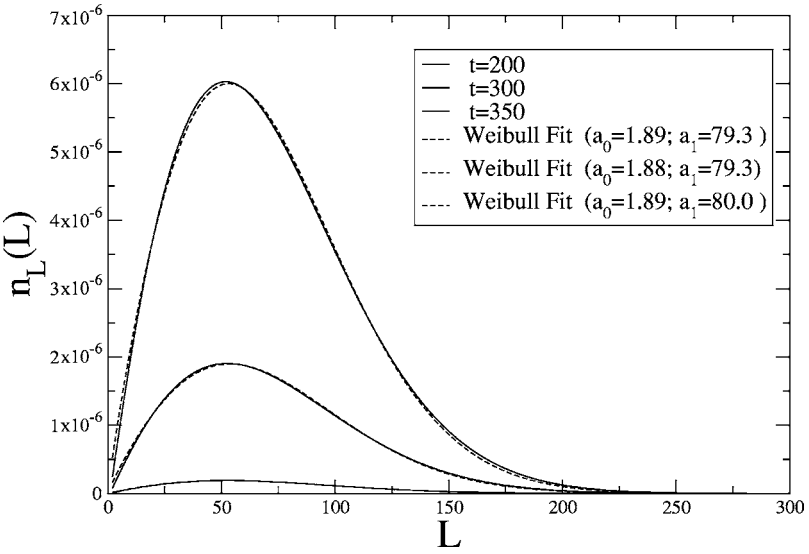

FIG. 4. Length distribution, n_l vs length L, from the kinetic equations during the exponential growth phase, compared with the Weibull distribution, Eq. (14).

qualitatively consistent with those observed experimentally displaying lengths in the tens of hundreds (see especially slide 9 at Ref. [10]). In Fig. 5, this mean length is plotted vs time for a different fission rate p_f. We see that the mean aggregate length is constant during the exponential growth. In Fig. 6, we show the variation of the exponential growth rate with p_f compared with the analytic calculations. One can see that they agree closely. Note also that p_f values of order 10^{-4} will give the lengths seen *in vitro*.

We can also determine the distribution of aggregate sizes in our calculations. The concentration of aggregates of different sizes relative to the initial concentration of monomers are shown in Fig. 4 for a given value of the fission parameter ($p_f=4\times10^{-4}$) at three different times during the exponential growth phase of the simulation. Clearly, the distribution is fairly stable during the exponential growth phase, further strengthening the argument for a simple steady state. These length distributions are well fitted by a Weibull distribution given by the relation,

$$f(x)=\frac{a_0}{a_1}\left(\frac{x}{a_1}\right)^{a_0-1}\exp\left[-\left(\frac{x}{a_1}\right)^{a_0}\right]. \tag{14}$$

Apart from an overall normalization, the two key parameters of the distribution are the mean a_1 and the power law at small x set by a_0-1. This distribution is found to be ubiquitous in nature [17]. For example, a dropped piece of coal will have shattered pieces that follow an asymmetrical distribution with more pieces on the smaller end. Our model follows a similar idea (i.e., taking a larger length and shattering it into smaller lengths) and a similar distribution. In our simulations, the quantity a_0 is close to 2 for a range of parameters studied. During subsequent times, the peak of this curve shifts to the left as saturation occurs and the only process left is to fission. (The shift in peak at later times are not shown here.)

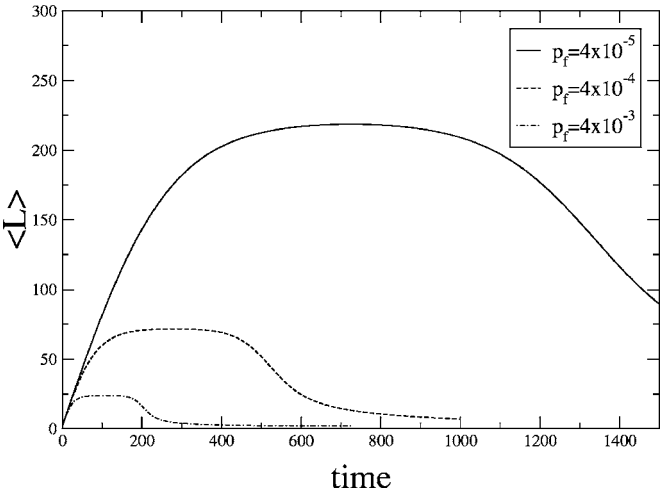

FIG. 5. Mean length vs time for different p_f; $n_1(0)=1$, $p_+=1$, $p_{nuc}=10^{-8}$. The plateau corresponds to the constant mean length during the exponential growth phase. Note that time is in units of $1/[n_1(0)p_+]$.

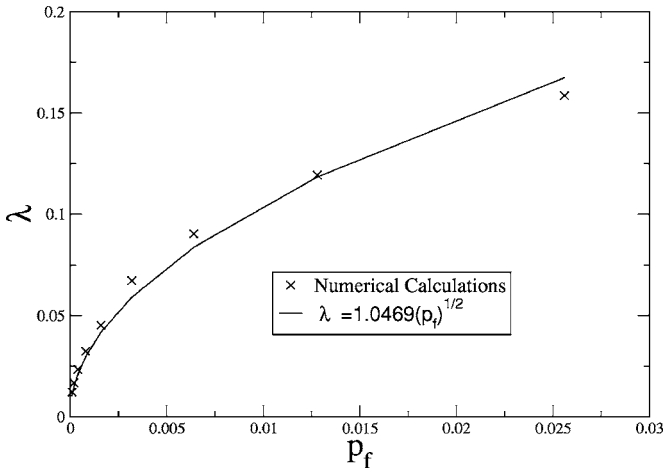

FIG. 6. Exponential growth rate λ vs p_f compared with simple square-root dependence predicted by Eq. (11) for different parameter values, $n_1(0)=1$, $p_+=1$, $p_{nuc}=10^{-8}$.

B. Comparison to nonfissioning micelle model

The coupling of the observation of weak concentration dependence with exponential growth strongly supports a model dominated by fissioning of aggregates constructed by monomer addition. Indeed, centrifugation studies confirm that monomers are the dominant species in the *in vitro* medium, and examination of the aggregation kinetics suggests a critical nucleus of small size [9].

It is thus important to contrast with other models for which a weak concentration dependence can be derived. Notably, the work of Lomakin *et al.* [11,12] considers kinetics with monomer growth of polymers as well as micellar oligomers composed of $\mathcal{M}$ monomers of concentration $n_{\mathcal{M}}$ which may or may not be off pathway. This model may be of relevance to other *in vitro* studies of yeast prion aggregation [18] for which there is evidence of oligomer formation and growth and a weak concentration dependence to the lag time. If the oligomers are off pathway, then assuming an equilibration with monomers leads to a buffering of the monomer concentration assuming an initially high input concentration and sufficiently rapid equilibration. There is a crossover or critical concentration n^* for this dictated by the equilibrium constant $K_{\mathcal{M}}$ between monomers and micelles ($K_{\mathcal{M}}=n_{\mathcal{M}}/n_1^{\mathcal{M}}$) given by

$$n^* = (\mathcal{M}K_{\mathcal{M}})^{1/1-\mathcal{M}}. \tag{15}$$

Lomakin *et al.* argue that for a total equilibrated protein concentration n_T obtained prior to fibril growth,

$$n_T = n_1 + \mathcal{M}n_{\mathcal{M}} \tag{16}$$

$$= n_1 + n^*\left(\frac{n_1}{n^*}\right)^{\mathcal{M}}. \tag{17}$$

From these equations, it is clear that there is an approximate two-state behavior provided $\mathcal{M} \gg 1$. For $n_T \ll n^*$, then $n_T \approx n_1$ and aggregation kinetics can be strongly concentration dependent. However, for $n_T \geqslant n^*$, then $n_1 \approx n^*$, that is, the micelles buffer the monomer concentration. This would lead to a weak dependence of fibrillar growth upon subsequent increase of initial monomer concentrations.

There are two routes by which this model can be applied to the data of Collins *et al.* [9,10]. First, if the fibrils are formed from monomer addition to the micelles without resulting fission of fibrils, then one will expect a quadratic growth in time [19,20] to the total number of aggregated proteins, namely

$$M(t) \approx \frac{1}{2}p_+^2 n_1^2 n_{\mathcal{M}} t^2, \tag{18}$$

$$\approx \frac{1}{2\mathcal{M}}p_+^2 n_1^{2+\mathcal{M}} (n^*)^{1-\mathcal{M}} n_{\mathcal{M}} t^2, \tag{19}$$

which is very weakly dependent upon $n_1(0)$ provided $n_1(0) \approx n_T \geqslant n^*$, but varies strongly as $n_1(0)^{2+\mathcal{M}}$ in the opposite limit. Solving for where $M(t_{lag})=M_c$ characteristic of the observability threshold yields

$$t_{lag} = \frac{1}{p_+ n_1}\sqrt{\frac{2M_c (n^*)^{\mathcal{M}-1}}{(n_1)^{\mathcal{M}}}}. \tag{20}$$

For $n_1(0) \ll n^*$, t_{lag} varies as $n_1(0)^{-(1+\mathcal{M}/2)}$, at odds with experiment [9], while for $n_1(0) \geqslant n^*$ and $\mathcal{M} \gg 1$, t_{lag} is approximately independent of $n_1(0)$ [it will decrease weakly with increasing $n_1(0)$].

Second, if the micelles are off pathway, then their principal impact on the fibrillar aggregation is on buffering. Assuming a critical fibrillar nucleus of length p, which equilibrates with the monomers via a constant $K_p=n_p/n_1^p$, the same considerations of aggregation kinetics as in the preceding paragraph give a lag time given by

$$t_{lag} = \frac{1}{p_+ n_1}\sqrt{\frac{2M_c}{K_p (n_1)^p}}. \tag{21}$$

For $n_1(0) \ll n^*$, this varies as $n_1(0)^{-(1+p/2)}$ is at odds with Collins *et al.* [9], while it is approximately independent of $n_1(0)$ for $n_1(0) \geqslant n^*$ and $p \gg 2$. For small nuclei ($p \simeq 2-5$, say), the dependence can be relatively strong on $n_1(0)$ even in this limit.

Hence, via either on-pathway or off-pathway micelles, in this model there is a route to weak dependence of lag time (defined as the threshold for observation) upon initial monomer concentration requiring $n_1(0) \geqslant n^*$ and $\mathcal{M}, p \gg 1$. However, there are several problems in connecting this to the experiments of Collins *et al.* First, exponential growth is unambiguously observed, indicating that fission of fibrils occurs. The micelle model of this subsection has no fission. This highlights the important role of fission for the prion phenomenon. Second, in these experiments, the starting solution contains almost entirely monomers and not micelles. This implies that even if micelles form, one is always in the limit of $n_1(0) \ll n^*$, leading to strong concentration dependence. Third, the width of the fibrils obtained in this experiment is apparently monomeric, which is not readily compatible with growth by monomer addition to micelles, and rather must be obtained by addition to a critical fibril nucleus. The data suggest that this critical fibril nucleus is of length $p \leqslant 6$, not consistent with the assumption $p \gg 1$.

Hence, we do not believe that the micelle based model can explain the data of Collins *et al.* [9,10].

C. Stochastic model

In this section, we develop a stochastic treatment of the model, similar to a model proposed by Pöschel *et al.* [21]. Our main motivation is to be able to treat species with small numbers, in which case the continuous deterministic approach will break down. As we will see, the stochastic approach largely agrees with the deterministic model for the parameter values considered here for aggregate quantities [e.g., $M(t)$]. However, for distributions there can be substantial stochastic noise at short times. Another advantage of the stochastic approach is that it can be readily extended to study

TABLE I. Propensities of stochastic processes.

Nucleation propensity	Fusion propensity for monomer addition		Higher order fusion term	Fission propensity for monomer		Higher order fission term
	Chain length 2	Chain length 3		Chain length 2	Chain length 3	
$g_{nuc}N_1(n_1-1)$	$2g_+N_1N_2$	$2g_+N_1N_3$	…	g_fN_2	$2g_fN_3$	…

two-dimensional aggregates as well as the problem of multiple prion "strains," in which case the treatment of a small number of heteroaggregates would be important to model the extent to which strains breed true.

The Gillespie algorithm provides an exact way to treat the stochastic problem of chemical reactions [22]. In our case, the polymers of different lengths are the different chemical species. The processes of nucleation, monomer addition, and fission are assumed to be stochastic. In other words, the number of polymers of different length at time t, only define the propensities (or normalized probability) for the different reactions to happen at that time. Once a reaction takes place, the number of polymers is altered and the propensities are changed. The Gillespie algorithm is a Monte Carlo treatment that deals with the stochastic process by using a pair of random numbers at each step, one to decide which event will occur next and another to decide how long will it be until the next event takes place. This process can be repeated to follow the dynamical behavior of the system.

Our model has the corresponding propensities

$$g_{nuc}N_1(N_1-1)+2g_+N_1\sum_{i=2}^{\infty}N_i+g_f\sum_{i=2}^{\infty}(i-1)N_i, \qquad (22)$$

where g_{nuc}, g_+, and g_f are, respectively, the nucleation, fusion, and fission parameters in the stochastic model. In our model, each propensity was assigned a bin in an array. A random number generator decides which bin is selected.

Table I illustrates physically the propensities at a given time. A normalized random number generator selects which element in the array will occur and the time it took to create that event. After an event occurs, the corresponding propensities are updated and the process is repeated.

In order to compare the results achieved from the continuous to stochastic model, a mapping of the Gillespie parameters to the kinetic parameters is required. For this, we need to develop an approximate equation satisfied by the monomer concentration in the stochastic simulations and compare it with the rate equations. In the stochastic case, one has a master equation that relates the probability distribution associated with a different number of polymers at time $t+dt$ to those at time t. We will make a mean-field approximation for different kind of k-mers, namely $\langle N_i * N_k\rangle = \langle N_i\rangle * \langle N_k\rangle$. Thus, we can consider the approximate master equation, which only tracks changes in the monomer number. We arrive at the equation,

$$\begin{aligned}P_1(N_1,t+dt) = P_1(N_1,t)\Bigg[1-g_{nuc}N_1(n_1-1)dt-g_+N_1\sum_{i=2}^{\infty}N_i dt \\ -2g_f\sum_{i=2}^{\infty}N_i dt\Bigg]+2P_1(N_1-1,t)g_f\sum_{i=3}^{\infty}N_i dt \\ +P_1(N_1-2,t)g_fN_2dt+P_1(N_1+1,t)g_+N_1 \\ \times\sum_{i=2}^{\infty}N_i dt+P_1(N_1+2,t)g_{nuc}N_1(N_1-1)dt,\end{aligned} \qquad (23)$$

where N_1 is the number of monomers, $P_1(N_1,t+dt)$ is the probability to have N_1 monomers at a later time $t+dt$. $P_1(N_1,t)$ is the probability to have N_1 monomers at time t. It is multiplied by the probability that no reaction occurs in time dt that changes N_1. The rest of the terms represent the probability to have a different number of monomers at time t but then a reaction happens in time dt leading to N_1 monomers at time $t+dt$.

Now using the definition of the derivative, one can rearrange the equation and multiply both sides by N_1 to get the average rate of change of N_1. After shifting some indices to get every probability to have the form $P_1(N_1,t)$ and using the appropriate volume element (denoted by V) to normalize the counts to a concentration, one arrives at the equation for the mean number of monomers,

$$\frac{1}{Vg_+}\frac{dn_1}{dt_{gil}} = -2g_{nuc}n_1^2-2n_1\sum_{i=2}^{\infty}n_i+2\frac{g_f}{V}\sum_{i=2}^{\infty}n_i. \qquad (24)$$

By comparing with the rate equations discussed before, we obtain the parameter mapping

$$p_+ = 1, \qquad (25)$$

$$p_{nuc} = g_{nuc}, \qquad (26)$$

$$p_f = \frac{g_f}{V}, \qquad (27)$$

$$t_{kinetic} = g_+Vt_{gillespie}. \qquad (28)$$

Results stochastic approach

After achieving the parameter mapping, we studied the stochastic models with 10^6 initial monomers. The numerical results are shown in the next few figures. In Fig. 7, the growth of the aggregate material is shown on a logarithmic

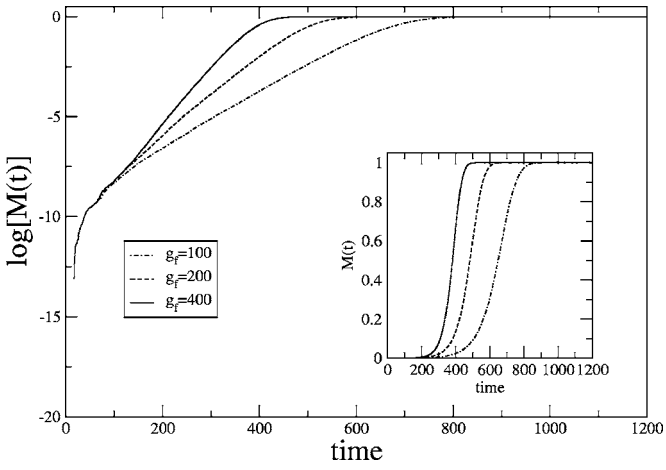

FIG. 7. Log$[M(t)]$ and $M(t)$, shown in the inset, vs time obtained by the Gillespie algorithm with $N_1(0)=10^6$, $g_+=1$, $g_{nuc}=10^{-8}$ for different fission rate g_f. Note that time is in units of $1/g_+$.

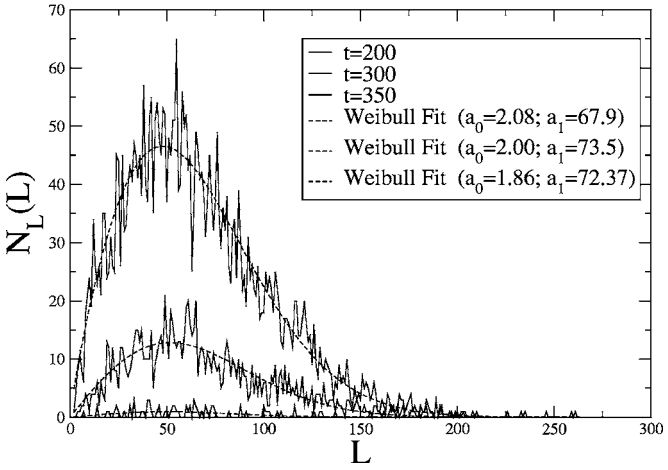

FIG. 9. Length distributions at different times during the exponential growth phase obtained by the Gillespie algorithm for $g_f=400$ and fitted by the Weibull distribution.

and on a linear scale. It is evident that they are in excellent agreement with the corresponding calculations for the kinetic model. In Fig. 8, we show plots of the mean length as a function of time, and in Fig. 9, the corresponding distribution of length scales during the exponential growth phase. It is again evident that there is a steady state during the exponential growth and the mean lengths reach a plateau value. The stochastic effects are much larger in the distribution and in the mean length, but the overall results agree well with the kinetic model. The fits to the Weibull distribution are again good with comparable parameters. The differences between the kinetic and stochastic Weibull parameters (a_0 and a_1) are less than 10%. This shows that for 10^6 monomers and for mean aggregate lengths up to a few hundred, the dominant species still occur in large enough numbers so that stochastic effects do not change the results in a significant way.

III. DISCUSSION

In this paper, we have used a deterministic kinetic and a stochastic Monte Carlo approach to model the dynamics of yeast prion growth. For the parameters relevant to *in vitro* experiments, where mean aggregate size is of order 100*s* of monomers, and the number of monomers is larger than 10^6, the two approaches agree well with each other, showing that stochastic effects are not dominant. The studies confirm that the key experimental features of the growth of yeast prions can be well captured by these nucleation-growth-fissioning models. They lead to an exponential and/or sigmoidal growth, an inverse square-root dependence of the lag time on the monomer concentration, and aggregate sizes that depend on the rate of fission. We predict that the aggregate size distributions should be Weibullian, reflecting the importance of fissioning in the growth process. We also predict, for sufficiently large times, that the steady state aggregate length will drop as fissioning converts large aggregates to those of minimal size. We have argued that models in which monomers equilibrate with micelles but do not fission [11,12], which are capable of producing lag times having a weak concentration dependence for a sufficiently high initial monomer concentration, are in fact not appropriate for the data of Collins *et al.* [9,10].

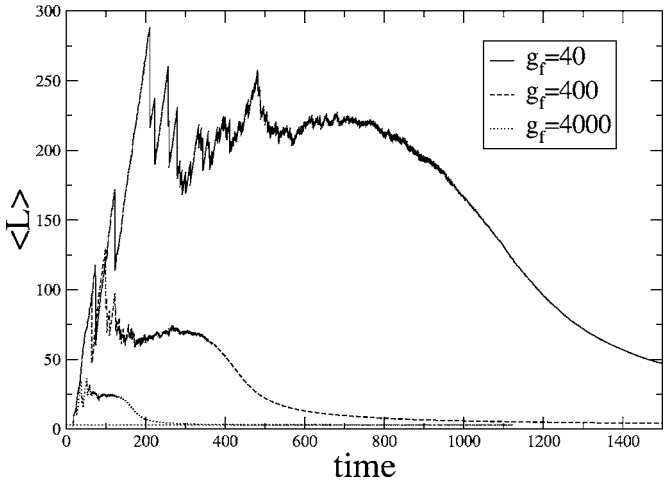

FIG. 8. Mean length vs time in units of $1/g_+$ for different fission rates g_f obtained by the Gillespie algorithm. The parameter values are $N_1(0)=10^6$, $g_+=1$, $g_{nuc}=10^{-8}$.

We note that the *in vitro* aggregation work of Serio *et al.* [18] appears to come to different conclusions than that of Collins *et al.* [9] and may be ripe for a discussion in terms of the micelle models. We do not understand the discrepancies between these two sets of experiments.

We note that the results on yeast prions discussed here and recent work on mammalian prions stripped of their GPI membrane anchors [23,24] suggest that a fundamentally different mechanism for fission is at play for the latter proteins *vis-à-vis* yeast. In the recent experiments, transgenic mice expressing the cellular prion protein without the residues necessary for the GPI anchor are exposed to anchorless infectious prions; in time course experiments, prion aggregates are produced which retain infectivity. However, the infected mice with anchorless PrP^C do not show clinical symptoms. Moreover, the time course data {see Fig. 1(c) of Chesebro *et al.* [24]} show two remarkable characteristics: (i) they are nonsigmoidal in shape, with the infectious prion content at long times significantly exceeding that of infected wild type

mice at death, (ii) the time scales to reach the levels of infectivity characteristic of wild type mice at the corresponding infectious dose are quite long. Indeed, the time course data can be fit roughly by a quadratic in time curve characteristic of nonfissioning aggregation to an initial concentration of infectious seeds. Evidently, the binding of cellular mammalian prions to the membrane is critical to the fissioning process, while for yeast prions fissioning of aggregates *in vitro* is observed [9].

In the future, we hope to extend this model to study yeast prion strains, where we expect the stochastic treatment to be the key to dealing with rare heteroaggregates. An understanding of this process should lead to insights into the important problem of strain dynamics in mammalian prions.

ACKNOWLEDGMENTS

We acknowledge the support of the U.S. Army Congressionally Mandated Biomedical Research Fund (Grant No. NP020132) and acknowledge the support of the NSF sponsored Center for Theoretical Biological Physics (NSF Grant Nos. PHY0216576 and 0225630). D.L.C. acknowledges the support of the J. S. Guggenheim Memorial Foundation.

[1] For a general introduction to prion biology, see S. B. Prusiner, *Prion Biology and Diseases*, 2nd ed. (C.S.H.L. Press, Cold Spring Harbor, NY, 2004).
[2] A. Aguzzi and M. Polymendiou, Cell **116**, 313 (2004).
[3] S. B. Prusiner, Science **216**, 136 (1982).
[4] G. Legname, I. Baskakov, H. Nguyen, D. Riesner, F. Cohen, S. DeArmond, and S. Pruisner, Science **305**, 673 (2004).
[5] R. B. Wickner, Science **264**, 566 (1994).
[6] H. E. Sparrer, A. Santosh, F. C. Szoka, Jr., and J. S. Weissman, Science **289**, 595 (2000).
[7] C. Y. King and R. Diaz-Avalos, Nature (London) **428**, 319 (2004).
[8] M. Tanaka, P. Chien, L. Z. Osherovich, and J. S. Weissman, Nature (London) **428**, 323 (2004).
[9] S. R. Collins, A. Douglass, R. Vale, and J. S. Weissman, PLoS Biol. **2**, 10 (2004).
[10] http://online.itp.ucsb.edu/online/bionet03/collins/
[11] A. Lomakin, D. S. Chung, G. B. Benedek, D. A. Kirschner, and D. A. Teplow, Proc. Natl. Acad. Sci. U.S.A. **93**, 1125 (1996).
[12] A. Lomakin, D. B. Teplow, D. A. Kirschner, and G. B. Benedek, Proc. Natl. Acad. Sci. U.S.A. **94**, 7942 (1997).
[13] A. Slepoy, R. R. P. Singh, F. Pazmandi, R. V. Kulkarni, and D. L. Cox, Phys. Rev. Lett. **87**, 058101 (2001).
[14] Holger Wille, Melissa D. Michelitsch, Vincent Guénebaut, Surachai Supattapone, Ana Serban, Fred E. Cohen, David A. Agard, and Stanley B. Prusiner, Proc. Natl. Acad. Sci. U.S.A. **99**, 3563 (2002).
[15] D. Hall and H. Edskes, J. Mol. Biol. **336**, 775 (2004).
[16] J. Masel, V. A. A. Jansen, and M. A. Nowak, Biophys. Chem. **77**, 139 (1999).
[17] W. Brown and K. Wohletz, J. Appl. Phys. **78**, 2758 (1995).
[18] T. R. Serio, A. G. Cashikar, A. S. Kowal, G. J. Sawicki, J. J. Moslehi, L. Serpell, M. F. Arnsdorf, and S. L. Lindquist, Science **289**, 1317 (2000).
[19] F. Ferrone, Methods Enzymol. **309**, 256 (1999).
[20] S. Chen, F. A. Ferrone, and R. Wetzel, Proc. Natl. Acad. Sci. U.S.A. **99**, 11884 (2002).
[21] T. Pöschel, N. V. Brilliantov, and C. Frömmel, Biophys. J. **85**, 3460 (2003).
[22] D. Gillespie, J. Comput. Phys. **22**, 403 (1976).
[23] P. Chien and J. Weissman, Nature (London) **410**, 223 (2001).
[24] B. Chesebro, M. Trifilo, R. Race, K. Meade-White, C. Teng, R. LaCasse, L. Raymond, C. Favara, G. Baron, S. Priola, B. Caughey, E. Masliah, and M. Oldstone, Science **308**, 1435 (2005).